

Anisotropy Induced Tunable Magnetic Properties of Chemically Synthesized Copper Ferrite ($\text{Cu}_x\text{Fe}_{1-x}\text{O}_4$) Nanoparticles with Different Composition

Pinaki Laha^{a*} & Rabindra Nath Gayen^b

^aDepartment of Physics, L.N.D. College, Motihari, B.R. Ambedkar Bihar University, Muzaffarpur, Bihar, 842 001, India

^bDepartment of Physics, Jadavpur University, Kolkata 700 032, India

Received 13 July 2023; accepted 1 November 2023

Here we report the structural and magnetic properties of cluster of ultrafine copper ferrite ($\text{Cu}_x\text{Fe}_{1-x}\text{O}_4$) nanoparticles with different Cu:Fe composition synthesized by aqueous chemical reduction technique. The morphological, microstructural and compositional studies confirm the formation of $\text{Cu}_x\text{Fe}_{1-x}\text{O}_4$ nanoparticles with varied Cu and Fe percentages which are polycrystalline in nature with fcc structure and average size of ~20 nm. Thermal stability and chemical purity of ferrite nanoparticles are ensured by analyzing the TGA/DTA curve in the temperature range 30-1000 °C. Magnetization vs magnetic field (M-H) hysteresis loops measured at two different temperatures (80K and 300K) reveal the typical ferromagnetic behavior of $\text{Cu}_x\text{Fe}_{1-x}\text{O}_4$ nanoparticles with a systematic change in the saturation magnetization (M_S), coercive field (H_C), remanent magnetization (M_r), Squareness (M_r/M_S), hardness (α) and effective anisotropy energy constant (K_{eff}) with the variation of Cu and Fe percentages. Tunable magnetic properties of ferrite nanoparticles with the variation of magnetic Fe and non-magnetic Cu are attributed to the modulation of effective anisotropy originated from the surface spin randomization.

Keywords — Soft magnetic materials; Ferrites; Nanoparticles; Magnetic properties

1 Introduction

The quest for innovative functional materials is a highly dynamic area of research, with a particular emphasis on transition metal oxides in the past two decades. These materials derive their unique properties from the interplay between transition metal and oxygen ions and making them highly responsive to variations in bond lengths and angles. As a result, within a single structural family, such as perovskite or spinel, one can discover a diverse array of materials exhibiting various physical phenomena¹⁻³. Ferrite nanoparticles with their unique magnetic properties have garnered immense research interest in recent time¹⁻¹⁰ driven by the promise of wide range of novel technological applications extended from ultrahigh density magnetic storage devices to the magnetic resonance imaging (MRI) technique, from biomedical nanotechnology to water treatment. All these applications are triggered by the static and dynamic magnetization properties of ferrite nanoparticles dispersed in different mediums. At nanoscale, magnetic properties of ultrafine particles are different from their bulk counterpart and controlled by size

effect and surface effect⁷⁻¹⁰. For dispersed nanoparticles, uniqueness of magnetic properties arises due to the coupling between neighbour particles, surface spin glass ordering, memory effects, collective phenomena and quantum tunnelling of magnetization^{11,12}. Nanostructured spinel ferrites [MFe_2O_4 (M = Co, Ni, Mn, Cu, Zn, etc.)] have obtained outstanding technological importance in recent times because of their interesting electrical, chemical and magnetic properties, with good thermal stability¹³. In particular, CuFe_2O_4 has also been very useful as a gas sensor, hydrogen production and as catalyst for CO_2 decomposition¹²⁻¹⁵ beside its usual magnetic applications. The synthesis of well dispersed magnetic ferrite nanoparticles has been a great challenge to the researchers due to higher rate of agglomeration of nano-sized magnetic particles. Various fabrication methods like solid-state reactions, advanced wet chemical methods, solvothermal methods, polymer-assisted sol-gel techniques^{5,6} etc. have been reported in recent times. However, most of the techniques are complicated with poor production rates and not so environment friendly. Also, there are few reports on the size and temperature dependent magnetic behaviour of spinel ferrite nanoparticles. But the detailed study on the dependence of magnetic

*Corresponding author:
(E-mail: lahapiinaki007@gmail.com)

properties on the composition of the constituents of spinel ferrite nanoparticles synthesized by relatively easy chemical reduction methods with high saturation magnetization value are scarce in the literature.

In this paper, we report the synthesis of $\text{Cu}_x\text{Fe}_{1-x}\text{O}_4$ nanoparticles with different composition of magnetic Fe and non-magnetic Cu by aqueous chemical reduction technique. The ultrafine nanoparticles are characterized by field emission scanning electron microscopy (FESEM), X-ray diffraction (XRD) technique, high resolution transmission electron microscopy (HRTEM) and thermo gravimetric analysis with differential thermal analysis (TGA/DTA). The magnetic properties of prepared $\text{Cu}_x\text{Fe}_{1-x}\text{O}_4$ samples are investigated by measuring magnetic hysteresis loops at 80 K and 300 K using a vibrating sample magnetometer (VSM). The anisotropy induced variation of magnetic properties of $\text{Cu}_x\text{Fe}_{1-x}\text{O}_4$ nanoparticles with Cu and Fe % is studied in detail which helps to understand the composition dependent magnetization in copper ferrite nanoparticles.

2. Experimental Details

Synthesis $\text{Cu}_x\text{Fe}_{1-x}\text{O}_4$ nanoparticles were synthesized by the slow chemical reduction method using 5 mM aqueous solutions of $\text{FeSO}_4 \cdot 7\text{H}_2\text{O}$ (Merck) and $\text{CuSO}_4 \cdot 5\text{H}_2\text{O}$ (Merck). Ratio of molar concentration of Fe and Cu salt was varied to obtain nanoparticles with different Cu: Fe composition. Then the mixture was stirred for 20 min and pH was adjusted to 7.0 with a 1M NaOH solution. Subsequently, 10 ml of a 10 mM aqueous solution of NaBH_4 was poured instantaneously with the mixture solution. A fine precipitate was obtained which was filtered magnetically. Then the precipitate was washed three times with de-ionised water and after that water was removed with the help of acetone. Here, Acetone was used as a dehydrating agent since it has a high solubility for water but not for the metal salts involved. Four different samples were obtained with four different compositions of Cu and Fe. With the increasing atomic percentage of Fe in the ferrite, four different samples have been presented as Sample 1 (28% Fe), Sample 2 (42% Fe), Sample 3 (65% Fe) and Sample 4 (72% Fe), in this study.

2.1 Characterizations

The morphology, crystal structure, composition, and particle size of the as prepared $\text{Cu}_x\text{Fe}_{1-x}\text{O}_4$ nanoparticles were studied using field emission scanning electron microscope (FESEM; Quanta FEG250), X-ray diffractometer (XRD; PANalytical

X'Pert PRO), energy dispersive x-ray spectrometer (EDX; Helios NanoLab, FEI), and transmission electron microscope (TEM; Helios NanoLab, FEI). The magnetization (M) with the applied magnetic field (H) was measured using a vibrating sample magnetometer (VSM; Lakeshore, model 7407). The simultaneous thermo gravimetry and differential thermal analysis (TGA/DTA) were carried out using a thermal analyser (Perkin Elmer, Diamond). The samples were heated from 30°C to 1100 °C in an inert atmosphere.

3 Results and Discussions

3.1 Microstructural and Compositional Studies

Figure 1 (a & b) show the FESEM images of the $\text{Cu}_x\text{Fe}_{1-x}\text{O}_4$ nanoparticles of Sample 1 and Sample 2, respectively in the powder form. The formation of ultrafine particles is apparent from the surface morphology, but they are agglomerated. For sample 2 that contains more Fe, agglomeration is more prominent.

The micro structural analysis of the samples is further carried out by TEM. The particles are dispersed in isopropanol using ultrasonic bath

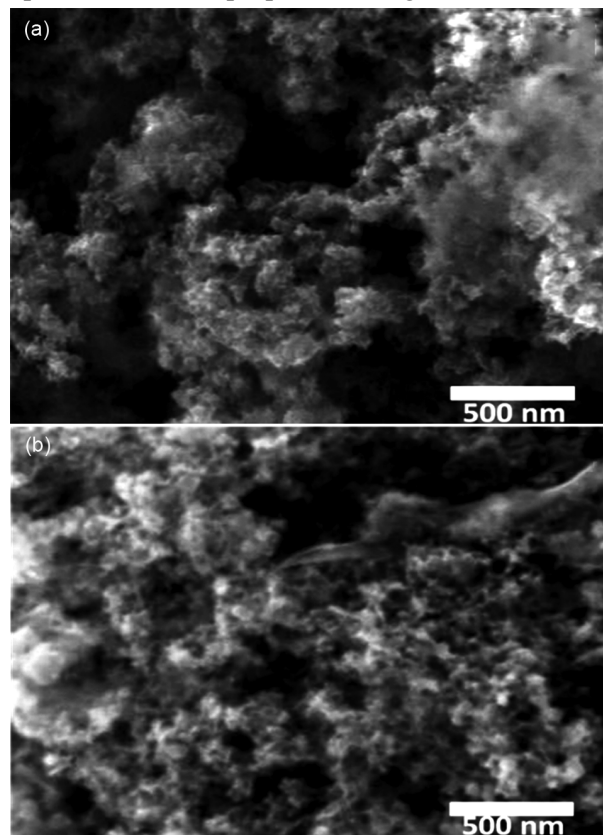


Fig. 1 — FESEM images of Cu-ferrite powder for (a) Sample 1 (Fe ~28%) and (b) Sample 2 (Fe ~42%).

sonicator before placing a drop of much diluted solution on the carbon coated copper grid for TEM measurement. Fig. 2(a) shows a representative TEM image of $\text{Cu}_x\text{Fe}_{1-x}\text{O}_4$ nanoparticles with less Fe content (Sample 1). It shows the well dispersed nanoparticles with almost spherical shape and average size of ~ 20 nm. The HRTEM image of Sample 1 (not shown here) shows the quasi-spherical shape of the single-phase nanoparticles with lattice spacing ~ 0.22 nm. The inset of Fig. 2 shows the selected area electron diffraction (SAED) pattern for all four samples. The results are indicating the fcc structure of the nanoparticles.

Insets of Fig. 2 (a-d) demonstrate the histogram of particle size distribution of the corresponding samples. From the peak position of the fitted Gaussian curve the formation of ultrafine grains with size in the range 7.2 nm to 13.8 nm are evident. Thus, TEM studies reveal the formation of polycrystalline nanoparticles of almost spherical shape.

Compositional analysis of the $\text{Cu}_x\text{Fe}_{1-x}\text{O}_4$ nanoparticles has been performed by EDX. To

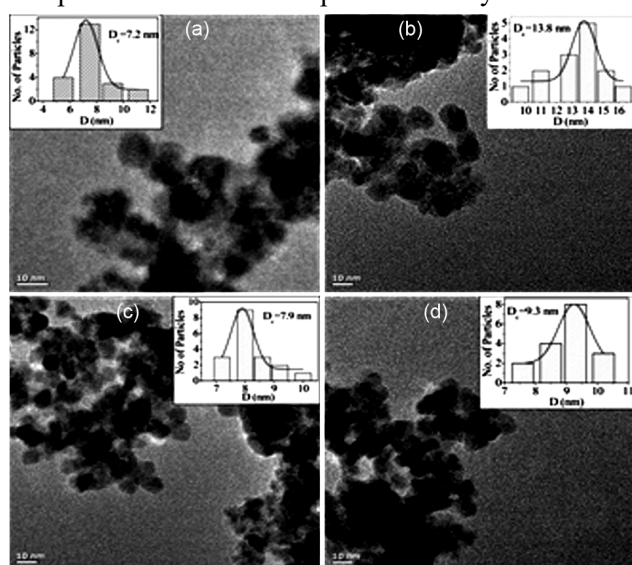


Fig. 2 — (a) TEM images of Cu-ferrite powder for Sample 1 (Fe \sim 28%), (b) Sample 2 (Fe \sim 42%), (c) Sample 3 (Fe \sim 65%) and (d) Sample 4 (Fe \sim 72%). Inset shows the histogram of particle distribution of corresponding sample.

confirm the uniformity of composition spot EDX analysis has been performed at different points of the nanoparticles. EDX spectra of $\text{Cu}_x\text{Fe}_{1-x}\text{O}_4$ nanoparticles with different Fe amount (Fig. 3 ((a-d))) confirm the presence of Fe, Cu and O indicating chemical purity of the ferrite nanoparticles. The amount of Cu and Fe (atomic percentage) present in different samples as obtained from the EDX analysis is tabulated in Table 1. The crystallinity and crystal structure of the powder samples are investigated by XRD pattern measured at room temperature using Cu- $\text{K}\alpha$ radiation of wavelength ~ 1.54 Å. Fig. 4 shows the XRD pattern of four different $\text{Cu}_x\text{Fe}_{1-x}\text{O}_4$ samples and exhibits several peaks corresponding to the characteristic reflections from (220), (311), (400), (422), (511), (440) and (533) planes of the spinel fcc crystal structure. The observed XRD peaks are in good agreement with the standard JCPDS card No. 77-001 for Cu ferrites. The polycrystalline nature of all the samples is evident from multiple strong

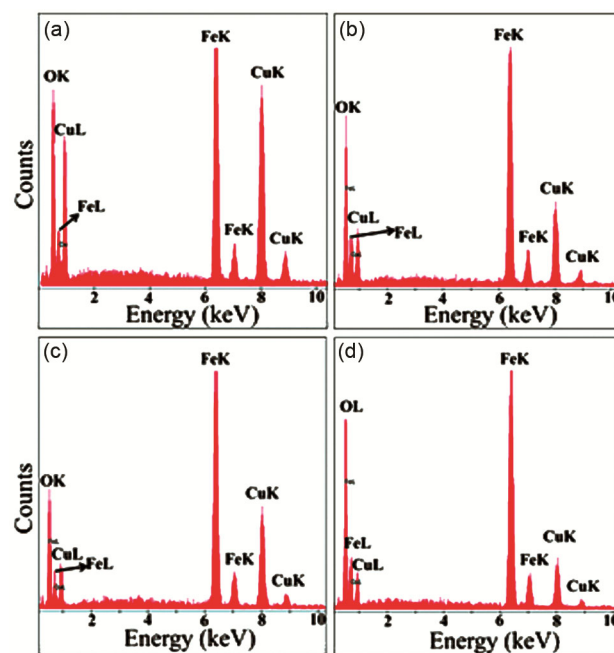


Fig. 3 — (a) EDX spectra of Cu-ferrite powder for Sample 1 (Fe \sim 28%), (b) Sample 2 (Fe \sim 42%), (c) Sample 3 (Fe \sim 65%) and (d) Sample 4 (Fe \sim 72%).

Table 1 — Calculated value of saturation magnetization (M_s), remanent magnetization (M_r), hardness (α) and coercive field (H_c) value of the samples from hysteresis loop.

Sample Name	Fe(%)	Cu (%)	D (nm)	M_s (emu gm^{-1})		H_c (Oe)		M_r (emu gm^{-1})		(M_r/M_s)		α	
				80K	300K	80K	300K	80K	300K	80K	300K	80K	300K
Sample 1	28	72	7.9	8.0	4.2	57	20	0.75	0.70	0.09	0.17	1953	3180
Sample 2	42	58	12.2	13.0	8.8	184	100	3.30	2.70	0.25	0.30	891	1089
Sample 3	65	35	8.8	32.0	25.1	140	38	6.00	4.50	0.19	0.18	860	1081
Sample 4	72	28	10.1	33.0	26.4	136	35	6.40	5.10	0.19	0.20	838	968

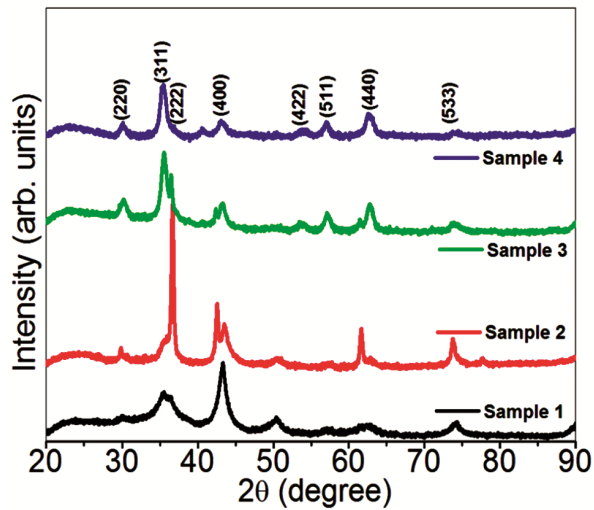


Fig. 4 — XRD pattern of ferrite nanoparticles with different composition of FE and Cu.

reflection peaks. Although the peak positions are not changed but the variation of relative intensities with increased Fe content in ferrite nanoparticles are attributed to the modification of unit cell parameters with different crystallographic orientations. The average grain size has been determined using Debye–Scherrer’s equation:

$$\beta = \frac{k\lambda}{L \cos \theta} \quad \dots(1)$$

where, λ is the wavelength of the Cu- K_{α} radiation, θ is the diffraction angle, k is the Scherrer constant which takes the value of 0.97 for spherical crystals with cubic symmetry, and L is the FWHM of the diffraction line corrected for the instrumental broadening. The crystallite size as estimated from the equation (1) is tabulated in Table -1.

3.2 TGA/DTA Studies

TGA/ DTA analysis of the synthesized samples have been studied in the temperature range from room temperature to 1100 °C to understand the thermal dependence of the samples. A ceramic (Al_2O_3) crucible was used for heating and measurements were carried out in a nitrogen atmosphere at the heating rate $10^{\circ}C \text{ min}^{-1}$. Fig. 5 (a & b) shows TGA/DTA curve for Sample 1 and Sample 2, respectively. It is apparent from the TGA curve that the ferrite nanoparticles continuously lose weight until 300°C with a total loss of 65%, which is attributed to vaporization of adsorbed water and the decomposition of Cu and Fe hydroxides from the sample. After that the rate of weight loss becomes slow up to 700 °C

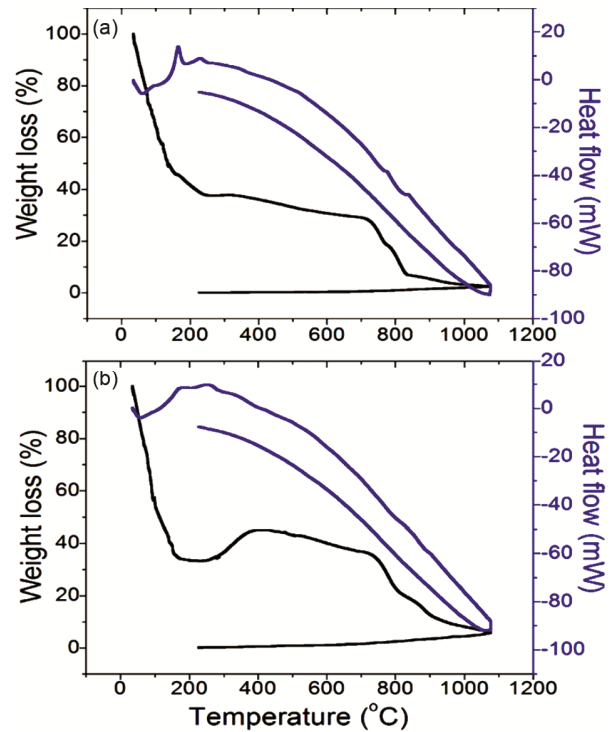


Fig. 5 — TG/DTA curve for (a) Sample 1 (Fe~ 28%) and (b) Sample 2 (Fe ~ 42%).

with a total loss of 5%. The second weight loss from 700 to 1100 °C attributed to the escape of oxygen atoms from the surface of nanoparticles. Correspondingly, DTA curves show an exothermic peak at 200 °C with a small exothermic peak at 300 °C due to the crystallisation of the sample. DTA profiles show that the complete thermal decomposition and crystallization of the samples occur simultaneously.

3.3 Magnetization Studies

Define The magnetic hysteresis loops for $Cu_xFe_{1-x}O_4$ have been obtained for four different samples at 80 K and 300 K. Fig. 6 (a & b) show the hysteresis curves of the synthesized samples at 80 K and 300 K, respectively. The magnetization values per gm of powder ferrite samples are measured with varied applied magnetic field. The hysteresis loops reveal a typical ferromagnetic nature of the as-synthesized $Cu_xFe_{1-x}O_4$. For all the samples, saturation occurs at fields of ~ 1000 Oe at 300 K, whereas at 80 K the samples are not magnetically saturated in that field. The reason for this difference can be explained by the magneto-electronic model. The difference in the saturation field is due to the para-process effect which is very small at 300 K. Lower coercivity (H_C) and

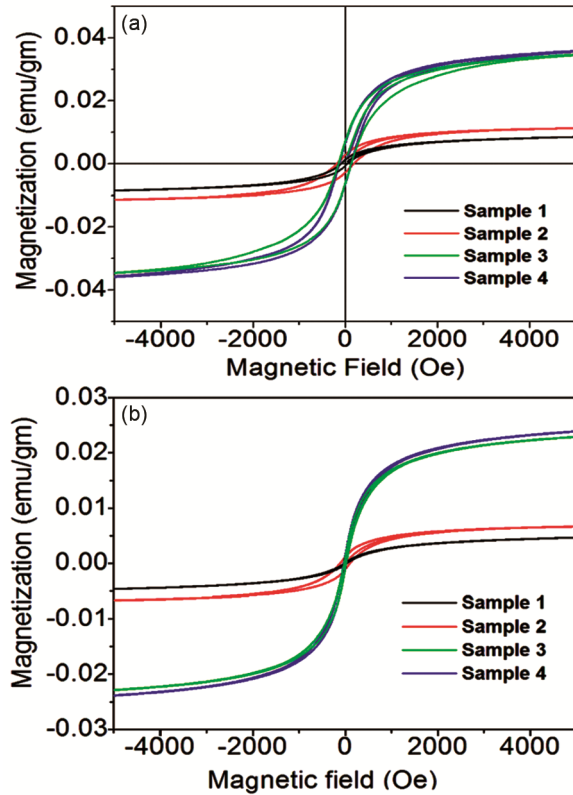


Fig. 6 — M-H curve of Cu ferrite nanoparticles measured at (a) 80K and (b) 300K.

saturation magnetization (M_S) values may be due to the strong anisotropy or inter-particle dipolar interaction in the strong magnetic system which can subdue the effects of surface spin values. Surface effect is associated with the broken exchange bonds and it lessens the coordination of surface cations and alter the super exchange near the surface. Magnetic properties in nanostructured materials are different from the bulk as the small size and surface play the major role. According to the core shell model, in spherical nanoparticles core is more magnetically ordered than shell. The presence of a magnetically dead layer on the surface of the nanoparticles or the presence of canted surface spins may be. In nanostructured magnetic particles the magnetization of the core is defined by how the spins are linked together to be in ordered state. The surface atoms have many broken exchange bonds that lead to the disordered surface spins. So, the particle magnetization loses its uniformity due to the disordered spins on the surface although the core is ordered. The temperature greatly affects this surface spin randomization to effectively control the magnetization of the particles. In Cu-ferrite

nanoparticles, the variation of composition of magnetic Fe and non-magnetic Cu affects the magnetization behaviour of the particles. The coercive field (H_c) and saturation magnetization values (M_S) as extracted from the M-H loops are presented in Table 1 for 80K and 300K. In addition, it is shown that the magnetization at 80K is larger than that of 300K as the thermal fluctuation is less and magnetic moments are aligned more orderly due to exchange interaction at 300K. At both the temperatures, the saturation magnetization (M_S) increases with the increase in magnetic Fe percentage in the ferrite nanoparticles. The presence of more Fe ion results in more ordered spin in the core and less randomization of surface spins. The coercive field (H_c) tends to increase with Fe content but not systematic with the variation of Fe content (Table 1).

The highest value of coercive field (H_c) is obtained for Sample 2 (Fe ~ 42%) due to the size effects as the particle size is larger. When the Fe content is significantly higher, the variation of M_S value is not so prominent. Due to the nano size, more atoms retain on the surface, which are not exchange coupled as a result of which the magnetic induction decreases¹⁶. The temperature effect of magnetization is also clear from this study. Both the values of saturation magnetization (M_S) and coercive field (H_c) are higher at low temperature (80 K) compared to the values at room temperature (300K) confirming the surface spin fluctuations due to thermal effects. The effective anisotropy constant (K_{eff}) of the $Cu_xFe_{1-x}O_4$ nanoparticles can be calculated from the Law of Approach to Saturation (LAS). It illustrates the dependence of magnetization (M) on the applied magnetic field (H) in the high magnetic field region ($H \gg H_c$). According to LAS, the magnetization near the saturation (M_S) can be expressed as¹³,

$$M = M_S \left(1 - \frac{b}{H^2} \right) \quad \dots(2)$$

where the parameter b is related with the effective anisotropy constant as:

$$K_{eff} = \mu_0 M_S \sqrt{\frac{15b}{4}} \quad \dots(3)$$

Using the experimental hysteresis loop, the value of b has been estimated from M versus $(1/H^2)$ linear plot (not shown here). From equation (3), K_{eff} values for Cu ferrite nanoparticles are calculated using the obtained value of b from the M versus $(1/H^2)$ plot.

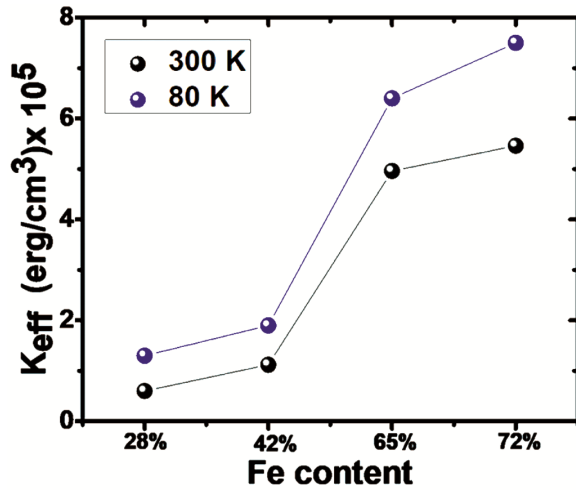


Fig. 7 — Variation of K_{eff} values with Fe% at 80 K and 300 K.

Disorder among surface spins is a dominant factor in the magnetic response of magnetic nanoparticle systems. In our case, the M_s value decreases with increasing temperature, which may be attributed to the reduction of surface spin layer thickness. Here, the LA model is implemented successfully for magnetization data at 80 K and 300 K both. So, we can say that temperature affects the surface spin randomization. Since the LA model accurately describes magnetization at high fields, from the M vs $1/H^2$ plot we can find out b parameter or slope by linear fitting which is different for 80 K and 300 K using eqn. 2.

Figure 7 shows the variation of effective anisotropy constant (K_{eff}) with the percentage of Fe in the ferrite nanoparticles. It is apparent from the figure that K_{eff} value significantly increases with Fe% in the Cu ferrite nanoparticles. The surface plays key role to induce large anisotropy value in magnetic nanoparticle. Generally, magnetic nanoparticles show a higher anisotropy value compared to their bulk counterpart attributed to the enhanced interaction and exchange bias effect between the core and surface spins. Saturation magnetization value of our sample ($D \sim 8.8$ nm) is higher than the previous researchers^{13,19}. If the squareness (M_r/M_s) value is greater than or equal to 0.5 then the nanoparticle is called as single domain structure but in this study squareness value is less than 0.5 which indicates the $Cu_xFe_{1-x}O_4$ nanoparticles are multi domain structure and possesses uniaxial anisotropy²⁰. The remanent magnetization (M_r) and squareness value of $Cu_xFe_{1-x}O_4$ nanoparticles with varying Cu and Fe composition are calculated and tabulated in Table 1.

Remanent magnetization (M_r) values of the samples increase with Fe % in copper ferrite nanoparticles. At the high magnetic field (H) region, the $M(H)$ curve can be described by the following relation²¹:

$$M = M_s \left(1 - \frac{\alpha}{H}\right) \quad \dots(4)$$

where, M_s is the saturated magnetization, H is external magnetic field and α is the measure of magnetic hardness of the particle. The hardness (α) value is calculated from the fitting procedure from the graph using the equation (4). It is clearly observed from Table 1 that α values are decreasing with Fe% in $Cu_xFe_{1-x}O_4$ nanoparticles. It indicates that $Cu_xFe_{1-x}O_4$ nanoparticles are changing from hard ferrite to soft ferrite with increasing Fe content in the sample. Also, the ultrafine magnetic nanoparticle shows the super paramagnetic behaviour which are attributed to the increased disorder of magnetic moments orientation in the various sites when the surface to volume ratio increases. Here the composition of Cu and Fe in ferrite samples plays the dominant role compared to the size effects in surface spin randomization which effectively tune the magnetic behavior as the variation in sizes are not significant.

4 Conclusion

Copper ferrite $Cu_xFe_{1-x}O_4$ nanoparticles with different compositions of Cu and Fe have been synthesized by aqueous chemical reduction route. Microstructural and compositional studies confirmed the formation of ferrite nanoparticles with spinel fcc crystal structures. Magnetic studies confirmed the dependence of magnetic properties on the composition of magnetic Fe and non-magnetic Cu in the ferrite nanoparticles. The modulation of magnetic properties of ultrafine Cu-ferrite nanoparticles are attributed to the anisotropy induced surface spin randomization which is controlled by composition of Fe and Cu content in the sample. The study of tunable magnetic properties with the compositional variation of Cu-ferrite nanoparticles is immensely important in the context of their application in the soft magnetic industry.

Acknowledgement

One of the authors, Pinaki Laha would like to acknowledge with thanks the support of B.R.A.B.U., Muzaffarpur in carrying out this work. R.N. Gayen

wish to acknowledge Jadavpur University for carrying out this work.

References

- 1 Kumar L & Kar M, *J Magn Magn Mater*, 323 (2011) 2042.
- 2 Rout S N, Manglam M K, Mallick J, Datta S, Kar M, *Physica B: Condensed Matter* 666 (2023) 415134.
- 3 Jasim A S, Patra I, Opulencia M J C, Hachem K, Parra R M R, Ansari M J, Jalil A T, Gazally M E A, Naderifar M, Khatami M & Sigari R A, *Nanotechnol Rev*, 11 (2022) 2483.
- 4 Masunga N, Mmelesi O K, Kefeni K K & Mamba B B, *J Environ Chem Eng*, 7 (2019) 103179.
- 5 Rosa J C I, Segarra M, *ACS Omega*, 4 (2019) 18289.
- 6 Kurian J, Mathew M J, *J Magn Magn Mater*, 451 (2018) 121.
- 7 Das B B, Venugopal P & Govinda R R, *Indian J Pure Appl Phys*, 53 (2015) 399.
- 8 Aquino R, Depeyrot J, Sousa M H, Tourinho F A, Dubois E & Perzynski R, *Phys Rev B*, 72 (2005) 184435.
- 9 Batlle X, Labarta A, *J Phys D*, 35 (2002) 469.
- 10 Kodama R H, *J Magn Magn Mater*, 200 (1999) 359.
- 11 Thomas L, Lioni F, Ballow R, Gatteschi D, Sessoli R & Barbara B, *Nature*, 383 (1996) 145.
- 12 Zhang X X, Hernandez J M, Tejada J & Ziolo R F, *Phys Rev B*, 54 (1996) 4101.
- 13 Mondal B, Kundu M, Mandal SP, Saha R, Roy U K, Roychowdhury A, *et al.*, *ACS Omega*, 4 (2019) 13845.
- 14 Chen N S, Yang X J, Liu E S & Huang J L, *Sens Actuators B: Chem*, 66 (2000) 178.
- 15 Shin H C, Choi S C, Jung K D & Han S H, *Chem Mater*, 13 (2001) 1238.
- 16 Nedelkoski Z, Kepaptsoglou D, Lari L, Wen T, Booth R A, Oberdick S D, Galindo P L, Ramasse Q M, Evans R F L, Majetich S & Lazarov V K, *Sci Rep*, 7 (2017) 45997.
- 17 Mameli V, Musinu A, Ardu A, Ennas G, Peddis D, Niznansky D, Sangregorio C, Innocenti C, Thanh N T K & Cannas C, *Nanoscale*, 8 (2016) 10124.
- 18 Kingery W D, Bowen H K & Uhlmann D R, *Introduction of Ceramics*, (New York: Willey) (1976) 993.
- 19 Chatterjee B K, Bhattacharjee K, Dey A, Ghosh C K & Chattopadhyay K K, *Dalton Trans*, 43 (2014) 7930.
- 20 Darwish M S A, Kim H, Lee H, Ryu C, Lee J & Yoon J, *Nanomaterials*, 9 (2019) 1176.
- 21 Cullity B D, *Introduction to Magnetic Materials*, (New York: Addison – Wesley) (1972).